Journal of Information Hiding and Multimedia Signal Processing ©2018 ISSN 2073-4212
Ubiquitous International Volume **9**, Number **5**, September **2018**

Research on The Transmission Characteristics of The I-shaped Deformation Ridge Waveguide

[1]Xia Zhao, and [2]Yong Zhou

[1]School of Automation and Electrical Engineering
[2]College of Continuing Education
[1,2]Lanzhou Jiaotong University, China

[1]zhaoxia@mail.lzjtu.cn

Received June, 2017; revised April, 2018

Abstract. *As a new kind of microwave component, the transmission characteristics of ridge deformation such as the cutoff-wavelength, the single-mode bandwidth, and the electrical field pattern in I-shaped ridge waveguide have been analyzed with the finite element method. Numerical results for different values of unilateral ridge deformation and bilateral ridge deformation have been presented in details. These data are helpful for the design and application of antipodal waveguide components.*
Keywords: I-shaped ridge waveguide; Finite element method; Transmission characteristics; Normalized cutoff wavelength; Single-mode bandwidth; Electrical field pattern

1. **Introduction.** Since the introduction of the ridge waveguide by Cohn in 1947[1], they have received considerable attention. Ridge waveguides have been widely used in the design of microwave and millimeter-wave devices because of their outstanding advantages: wider single-mode broadband, longer dominant cutoff wavelength, and lower impedance characteristics, etc.[2].

However, in the process of manufacture, assembly, and use, the deformation of ridge waveguide is unavoidable. Study of the influence of ridge deformation on the transmission characteristics is helpful for analysis of the microwave devices and system more scientifically and exactly. A variety of ridge waveguides have been analyzed in literatures [3-7]. Thus, this paper mainly discusses the transmission characteristics of I-shaped waveguide in different ridge deformations with the finite element method (FEM)[8].

2. **Theoretical Analysis.** Assume the medium in the ridge waveguide is air, and the air is uniform in the longitudinal direction. Based on the longitudinal field method and $\emptyset$ in place of H_Z, the field of the waveguide can be reduced precisely to find a scalar function, given by

$$\frac{\partial^2 \emptyset}{\partial x^2} + \frac{\partial^2 \emptyset}{\partial y^2} + k_c^2 \emptyset = 0 \tag{1}$$

Where $k_c^2 = k^2 - \beta^2 = \omega^2 \mu\varepsilon - \beta^2$, ε and μ are the permittivity and permeability respectively, and β is the phase constant representing the wavelength of guide.

The dominant TE mode satisfies the Helmholtz equation with Neumann boundary condition over the cross section of the guide. According to the variational principle, the above problem is equivalent to the following variational problem:

$$F(\emptyset) = \frac{1}{2}\iint_{\Omega}\left\{\left[\frac{\partial\emptyset}{\partial x}\right]^2 + \left[\frac{\partial\emptyset}{\partial y}\right]^2 - k_c^2\emptyset\right\}d\Omega \tag{2}$$

Where Ω is the section area of waveguide.

The cross section of the ridge waveguide is divided into a number of triangular elements by using the FEM. The linear interpolation method is used to analyze each triangular element of the whole field. Then the characteristic values and other electric parameters of the ridge waveguide can be obtained.

By the linear interpolation, $\emptyset_n$ of triangular element can be expressed as the following equation:

$$\emptyset_n(x,y) = \sum_{j=1}^{3} N_j^n(x,y)\emptyset_j^n \tag{3}$$

In this expression, $\emptyset_1^n$, $\emptyset_2^n$, $\emptyset_3^n$ respectively represent the values of the field $\emptyset$ in the corresponding nodal points, $N_j^n(x,y)\emptyset_j^n$ is interpolation function.

The TE mode in the ridge waveguide satisfies the Neumann boundary condition, which can satisfy Eq.(2) automatically. Plug the Eq.(3) into the Eq.(2), then the matrix problem can be written as Eq.(4) by using the differentiation.

$$\left[\frac{\partial^n F}{\partial\emptyset^n}\right] = [K^n]\,[\emptyset^n] \tag{4}$$

where $\left[\frac{\partial^n F}{\partial\emptyset^n}\right] = \left[\frac{\partial^n F}{\partial\emptyset_1^n}, \frac{\partial^n F}{\partial\emptyset_2^n}, \frac{\partial^n F}{\partial\emptyset_3^n}\right]^T$, $[\emptyset^n] = [\emptyset_1^n, \emptyset_2^n, \emptyset_3^n]^T$

All units are assembled. Then the following equation is obtained:

$$\left[\frac{\partial F}{\partial\emptyset}\right] = \sum_{n=1}^{q}\left[\frac{\partial^n F}{\partial\emptyset^n}\right] = \sum_{n=1}^{q}[K^n]\,[\emptyset^n] = 0 \tag{5}$$

The above equation can be simplified as the following matrix problem:

$$[K]\,[\emptyset] = 0 \tag{6}$$

Where $[K]$ consist of $[K^n]$, $[\emptyset]$ are the column vector.

$[K]$ are the eigenvalues which represent the cutoff frequency. The minimum and nonnegative eigenvalue is the cutoff frequency of the dominant TE mode, which is represented as k_c. The second minimum and nonnegative eigenvalue is the cutoff frequency of the first higher-order TE mode. Thus, the cutoff wavelength and the single-mode bandwidth can be easily obtained from the Eq.(7) and the Eq.(8).

$$\lambda_c = \frac{2\pi}{k_c} \tag{7}$$

$$BW = \lambda_{c1}/\lambda_{c2} \tag{8}$$

3. **Numerical Results.** The cross section of the I-shaped ridge waveguide is shown in Fig.1. a and b are the outer dimensions of the waveguide respectively. s is the ridge width. The parameters c, t, h and d are used to measure the ridge position. The basic geometrical parameter used in the calculations is selected as $b/a = 0.45$.

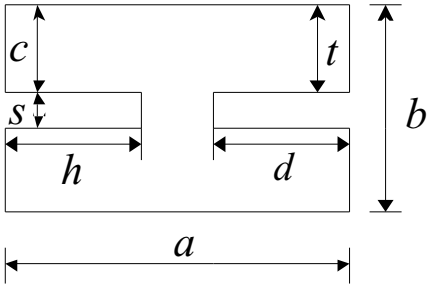

FIGURE 1. Cross section of the I-shaped ridge waveguide

The task to find the solution of field patterns with different ridge positions is certainly vast. Limited by the following size of this paper, only the dominant TE mode and the first higher-order TE mode are presented.

TABLE 1. Normalized cutoff wavelength of the dominant TE mode for $c/b = 0.1, 0.2, 0.3, 0.4$ with different h/a

c/b	h/a					
	0.1	0.2	0.3	0.4	0.5	0.6
0.1	1.8042	1.7746	1.8108	1.9949	2.3884	2.9128
0.2	1.8037	1.7651	1.7888	2.0717	2.5015	3.1033
0.3	1.8028	1.7618	1.7693	2.0999	2.5463	3.1874
0.4	1.8029	1.7639	1.7898	2.0681	2.5020	3.0993

TABLE 2. Single-mode bandwidth for $c/b = 0.1, 0.2, 0.3, 0.4$ with different h/a

c/b	h/a					
	0.1	0.2	0.3	0.4	0.5	0.6
0.1	1.0800	1.0585	1.0773	1.1044	1.2296	1.4235
0.2	1.0766	1.0510	1.0449	1.1318	1.3006	1.5553
0.3	1.0781	1.0494	1.0151	1.1444	1.3261	1.6041
0.4	1.0773	1.0517	1.0447	1.1313	1.3006	1.5537

Table 1 and Table 2 respectively show the data of normalized cutoff wavelength and single-mode bandwidth of the dominant TE mode for fixed $s/b = 0.4, t/b = 0.3, d/a = 0.3$. Fig.2 to Fig.5 respectively demonstrate the field patterns of the dominant TE mode and the first higher-order TE mode in I-shaped ridge waveguide for the unilateral deformation. The main results are as follows.

1. For fixed h/a on 0.1, 0.2 or 0.3, the normalized cutoff wavelength decreases first and then increases as c/b increases from 0.1 to 0.4, and the minimum value can be obtained when c/b is 0.3. For fixed h/a on 0.4, 0.5 or 0.6, the normalized cutoff

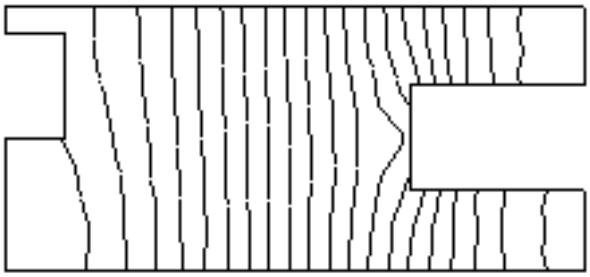

FIGURE 2. Electrical field pattern of the dominant TE mode for $h/a = 0.1, c/b = 0.1$

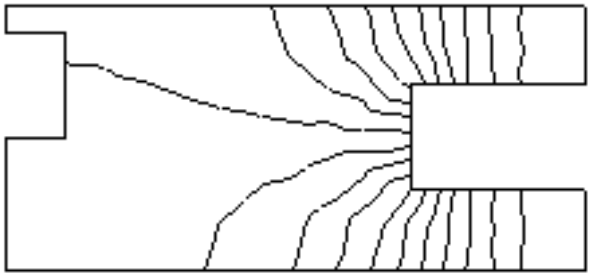

FIGURE 3. Electrical field pattern of the first higher-order TE mode for $h/a = 0.1, c/b = 0.1$

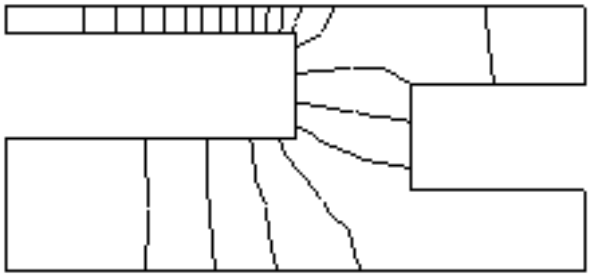

FIGURE 4. Electrical field pattern of the dominant TE mode for $h/a = 0.5, c/b = 0.1$

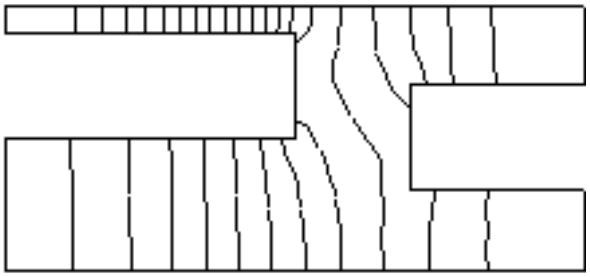

FIGURE 5. Electrical field pattern of the first higher-order TE mode for $h/a = 0.5, c/b = 0.1$

wavelength increases first and then decreases as c/b increases from 0.1 to 0.4, and the maximum value can be obtained when c/b is 0.3. For fixed c/b, the normalized cutoff wavelength decreases first and then increases as h/a increases from 0.1 to 0.6, and the minimum value can be obtained when h/a is 0.2.

2. For fixed h/a on 0.2 or 0.3, the single-mode bandwidth decreases first and then increases as c/b increases from 0.1 to 0.4, and the minimum value can be obtained when c/b is 0.3. For fixed h/a on 0.4, 0.5 or 0.6, the single-mode bandwidth increases first and then decreases as c/b increases from 0.1 to 0.4, and the maximum value can be obtained when c/b is 0.3. For fixed c/b, the single-mode bandwidth decreases first and then increases as h/a increases from 0.1 to 0.6.
3. In the field figures, the density of the lines indicates the relative strength of the electric field. The electrical field of the dominant TE mode and the first higher-order TE mode are very well concentrated in the invariant ridge area for h/a=0.1, c/b=0.1. The electrical field of the dominant TE mode and the first higher-order TE mode are few and scattered, and very well concentrated in the variant ridge area for h/a=0.5, c/b=0.1.

TABLE 3. Normalized cutoff wavelength of the dominant TE mode for $c/b(t/b) = 0.1, 0.2, 0.3$ with different $h/a(d/a)$

$c/b(t/b)$	$h/a(d/a)$				
	0.1	0.2	0.3	0.4	0.45
0.1	1.8495	1.7723	1.8151	2.0668	2.5110
0.2	1.8456	1.7559	1.7839	2.2630	2.8061
0.3	1.8446	1.7520	1.7693	2.3254	2.9260

TABLE 4. Single-mode bandwidth for $c/b(t/b) = 0.1, 0.2, 0.3$ with different $h/a(d/a)$

$c/b(t/b)$	$h/a(d/a)$				
	0.1	0.2	0.3	0.4	0.45
0.1	1.8508	1.4478	1.1506	1.0727	1.2734
0.2	1.8185	1.3447	1.0486	1.1873	1.4304
0.3	1.7968	1.3100	1.0151	1.2335	1.4984

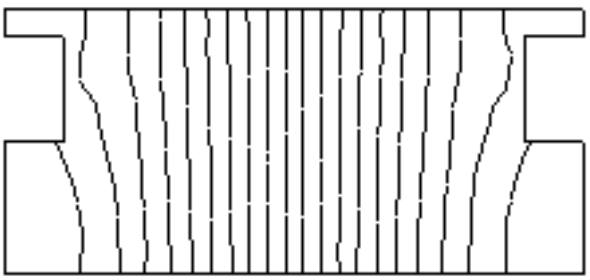

FIGURE 6. Electrical field pattern of the dominant TE mode for $h/a(d/a) = 0.1, c/b(t/b) = 0.1$

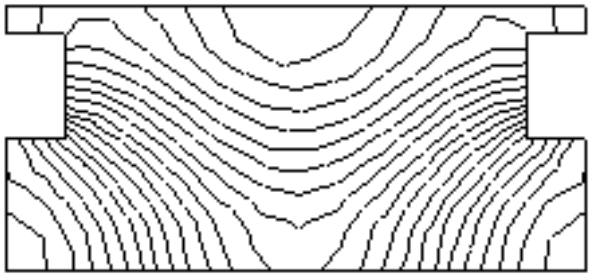

FIGURE 7. Electrical field pattern of the first higher-order TE mode for $h/a(d/a) = 0.1, c/b(t/b) = 0.1$

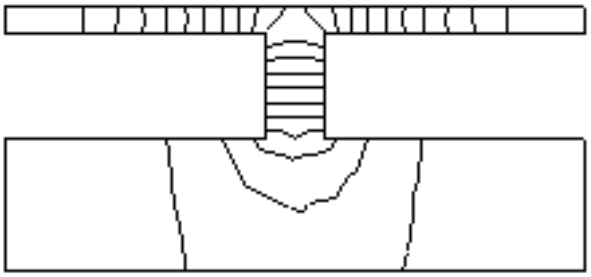

FIGURE 8. Electrical field pattern of the dominant TE mode for $h/a(d/a) = 0.45, c/b(t/b) = 0.1$

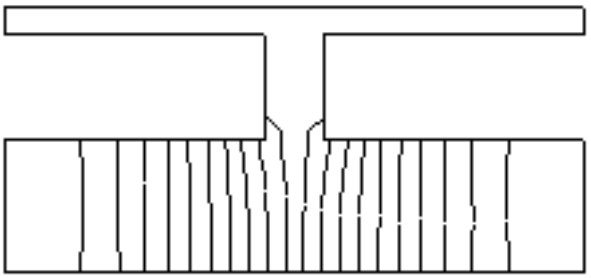

FIGURE 9. Electrical field pattern of the first higher-order TE mode for $h/a(d/a) = 0.45, c/b(t/b) = 0.1$

Table 3 and Table 4 respectively show the data of normalized cutoff wavelength and single-mode bandwidth of the dominant TE mode for fixed $s/b = 0.4, t = c, d = h$. Fig.6 to Fig.9 respectively demonstrate the field patterns of the dominant TE mode and the first higher-order TE mode in I-shaped ridge waveguide for the bilateral deformation with the same direction. The main results are as follows.

1. For fixed $h/a(d/a)$ on 0.1, 0.2 or 0.3, the normalized cutoff wavelength decreases as $c/b(t/b)$ increases from 0.1 to 0.3. For fixed $h/a(d/a)$ on 0.4 or 0.45, the normalized cutoff wavelength increases as $c/b(t/b)$ increases from 0.1 to 0.3. For fixed $c/b(t/b)$, the normalized cutoff wavelength decreases first and then increases as $h/a(d/a)$ increases from 0.1 to 0.45, and the minimum value can be obtained when $h/a(d/a)$ is 0.2.

2. For fixed $h/a(d/a)$ on 0.1, 0.2 or 0.3, the single-mode bandwidth decreases as $c/b(t/b)$ increases from 0.1 to 0.3. For fixed $h/a(d/a)$ on 0.4 or 0.45, the single-mode bandwidth increases as $c/b(t/b)$ increases from 0.1 to 0.3. For fixed $c/b(t/b)$, the normalized cutoff wavelength decreases first and then increases as $h/a(d/a)$ increases from 0.1 to 0.45.
3. The electrical field of the dominant TE mode and the first higher-order TE mode are symmetrical and evenly distributed in the ridge area for $h/a(d/a)$=0.1, $c/b(t/b)$=0.1. For $h/a(d/a)$=0.45, $c/b(t/b)$=0.1, the electrical field of the dominant TE mode is very well concentrated in the narrow ridge area, and the electrical field of the first higher-order TE mode is very well concentrated in the wide ridge area.

TABLE 5. Normalized cutoff wavelength of the dominant TE mode for $c/b = 0.1, 0.2, 0.3$ and $t/b = 0.5, 0.4, 0.3$ with different $h/a(d/a)$

$c/b(t/b)$	$h/a(d/a)$				
	0.1	0.2	0.3	0.4	0.45
0.1(0.5)	1.8497	1.7777	1.8527	2.1763	2.5240
0.2(0.4)	1.8458	1.7566	1.8109	2.2633	2.7895
0.3(0.3)	1.8446	1.7520	1.7693	2.3254	2.9260

TABLE 6. Single-mode bandwidth for $c/b = 0.1, 0.2, 0.3$ and $t/b = 0.5, 0.4, 0.3$ with different $h/a(d/a)$

$c/b(t/b)$	$h/a(d/a)$				
	0.1	0.2	0.3	0.4	0.45
0.1(0.5)	1.9026	1.4981	1.2164	1.1905	1.2878
0.2(0.4)	1.8310	1.3562	1.0895	1.2093	1.4242
0.3(0.3)	1.7968	1.3100	1.0151	1.2335	1.4984

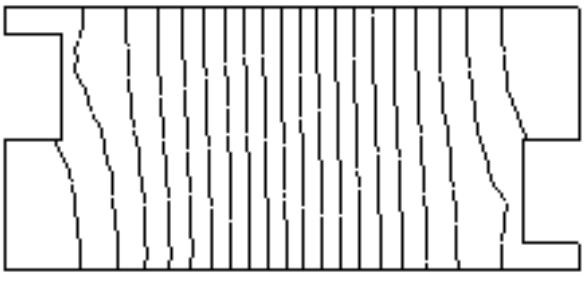

FIGURE 10. Electrical field pattern of the dominant TE mode for $h/a(d/a) = 0.1, c/b = 0.1, t/b = 0.5$

Table 5 and Table 6 respectively show the data of normalized cutoff wavelength and single-mode bandwidth of the dominant TE mode for fixed s/b=0.4, $d = h$. Fig.10 to Fig.13 respectively demonstrate the field patterns of the dominant TE mode and the first higher-order TE mode in I-shaped ridge waveguide for the bilateral deformation with the opposite direction. The main results are as follows.

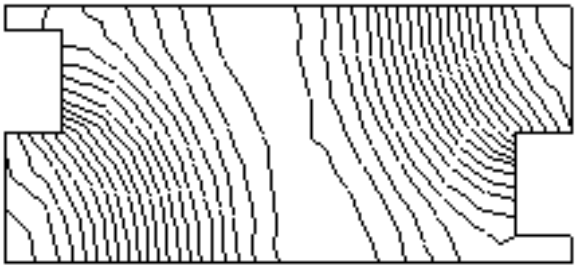

FIGURE 11. Electrical field pattern of the first higher-order TE mode for $h/a(d/a) = 0.1, c/b = 0.1, t/b = 0.5$

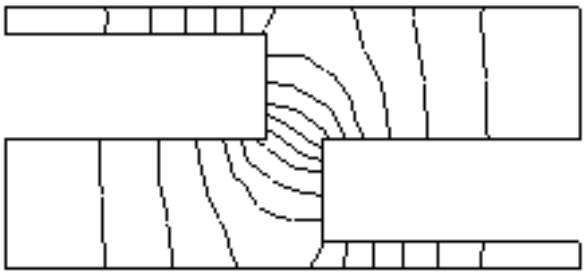

FIGURE 12. Electrical field pattern of the dominant TE mode for $h/a(d/a) = 0.45, c/b = 0.1, t/b = 0.5$

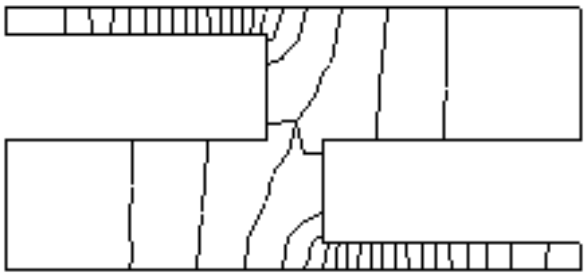

FIGURE 13. Electrical field pattern of the first higher-order TE mode for $h/a(d/a) = 0.45, c/b = 0.1, t/b = 0.5$

1. For fixed $h/a(d/a)$ on 0.1, 0.2 or 0.3, the normalized cutoff wavelength decreases as c/b increases from 0.1 to 0.3. For fixed $h/a(d/a)$ on 0.4 or 0.45, the normalized cutoff wavelength increases as c/b increases from 0.1 to 0.3. For fixed c/b and t/b, the normalized cutoff wavelength decreases first and then increases as $h/a(d/a)$ increases from 0.1 to 0.45, and the minimum value can be obtained when $h/a(d/a)$ is 0.2.
2. For fixed $h/a(d/a)$ on 0.1, 0.2 or 0.3, the single-mode bandwidth decreases as c/b increases from 0.1 to 0.3. For fixed $h/a(d/a)$ on 0.4 or 0.45, the single-mode bandwidth increases as c/b increases from 0.1 to 0.3. For fixed c/b and t/b, the normalized cutoff wavelength decreases first and then increases as $h/a(d/a)$ increases from 0.1 to 0.45.
3. The electrical field of the dominant TE mode and the first higher-order TE mode are symmetrical and evenly distributed in the ridge area, and are very well concentrated in the ridge area.

4. **Conclusion.** The cutoff wavelength, the single-mode bandwidth and the field patterns are presented by finite element method in I-shaped waveguide of the unilateral ridge deformation and the bilateral ridge deformation. The figures in this paper are useful in the design of the components for broadband microwave transmission.

Acknowledgment. Project supported by Youth Foundation of Lanzhou Jiaotong University (2014035); Opening Foundation of Key Laboratory of Opto-Technology and Intelligent Control Ministry of Education (Lanzhou Jiaotong University)(KFKT2016-1).

REFERENCES

[1] S. B. Cohn, Properties of ridge waveguide, *Proc. IRE*, vol. 35, pp. 783-788, 1947.
[2] X. Zhao , X.-q. Chen, M. Lu, E.-e. Ren, Study of transmission characteristic of trapezoidal-ridge waveguide in different distortions, *Laser & Infrared*, vol. 38, pp. 590-592, 2008.
[3] M. Farid Shah, Design and analysis of multiple ridge waveguide for wideband application, *Proceedings of 2014 IEEE International Conference on Advanced Communication, Control and Computing Technologies*, pp. 886-890, 2015.
[4] H. Zhang, Study on the ridge grooves deformation of double-ridged waveguide tube in rotary draw bending based on analytical and simulative methods, *Journal of Materials Processing Technology*, vol. 243, pp. 100-111, 2017.
[5] X. Zhao, X.-q. Chen, Eigenvalue analysis of triangle- ridge waveguide in deformation on finite element method, *Laser Journal*, vol. 33, pp. 9-10, 2012.
[6] J. Lei, X. Chen, Q. Yang, Study on transmission characteristics of the dielectric loaded asymmetric inverted trapezoidal single ridge waveguide, *Semiconductor Optoelectronics*, pp. 665-669, 2017.
[7] X. Chen, L. Yang, Transmission characteristics of triangle ridge waveguide in combined deformations, *Laser & Infrared*, pp. 1244-1248, 2015.
[8] J. Jin, Electromagnetic FEM, *Xidian University Press*, 2001.